

RADICAL STABILIZATION OF MESO PORPHYRINOIDS. GLEANNING THEORETICAL DATA FOR THE RATIONAL DESIGN OF PORPHYRINYL PRODRUGS

BÁRBARA GORDILLO-ROMÁN*

(Received September 2012; Accepted November 2012)

This paper is dedicated to Professor Pedro Joseph-Nathan in recognition of his 50 years of outstanding scientific trajectory.

ABSTRACT

This article is engaged with the search for a confident theoretical model to study the stabilization energies and geometry of free radicals stabilized by a porphin ring and/or a *p*-X-substituted phenyl ring, where X is either an electron donating or withdrawing atom or group. DFT calculations at the B3LYP/6-31G(d,p) or UB3LYP/6-31G(d,p) levels of theory were applied to homolog series of saturated porphyrins **2(a-h)** - **5(a-h)** and porphyrinoids **3(a-h)**, **4(a-h)** series, respectively. Calculated radical stabilization energy (RSE) values for the various *p*-X-phenyl substituents of benzyl radical **6(a-h)** series obtained through an isodesmic reaction model (Scheme 1) provided a quite good correlation ($r = 0.989$) with the radical total effect (TE) reported by Wu (Wu *et al.*, 1996). The TE effect is generally accepted as a scale to study radical stabilization due to spin delocalization, since it is in a very good agreement with the experimental ESR hyperfine coupling constants (hfc) of benzyl radicals (Dust and Arnold, 1983). Likewise, isodesmic RSE values for porphyrinoid **3(a-h)** series provided a good correlation ($r = 0.940$) with RSE values for **6**. However, RSE values for porphyrinoid **4β(a-h)** series deviate from the expected correlation trend ($r = 0.731$), not to mention **4α(a-h)** series ($r = 0.660$). Relative absorption wavenumbers ($\Delta\lambda$, nm) at the λ_{\max} bands of porphyrin series [$\lambda(\mathbf{3}^{\cdot}) - \lambda(\mathbf{3})$] and [$\lambda(\mathbf{4}^{\cdot}) - \lambda(\mathbf{4})$] indicate large porphyrinoid bathochromic effects (*ca.* 200 - 300 nm). www.relaquim.com

Keywords: porphyrin, theoretical calculations, free radicals, bathochromic effect.

RESUMEN

Este artículo está comprometido con la búsqueda de un método confiable para estudiar las energías de estabilización y geometría de radicales libres estabilizados por un anillo de porfina y/o un fenilo *p*-sustituido con grupos X, donde X es un átomo o grupo electrodonador o electroattractor. El método DFT a nivel de teoría

Departamento de Química, Centro de Investigación y de Estudios Avanzados del Instituto Politécnico Nacional, Apartado 14-740, México, D. F., 07000 México.

* Correspondance should be addressed to ggordill@cinvestav.mx. Tel: +52(55)5747-3729. Fax: +52(55)5747-3389.

B3LYP/6-31G(d,p) o UB3LYP/6-31G(d,p) se usó para simular las series de porfirinas **2(a-h)** - **5(a-h)** y de porfirinoides **3(a-h)**, **4(a-h)**, respectivamente. Los valores de la energía de estabilización de radicales (RSE) se obtuvieron por medio de una reacción isodésmica modelo, aplicada a los radicales bencílicos sustituidos en posición *para* con grupos X **6(a-h)** dando una buena correlación con los valores del efecto total de radicales (TE) informado por Wu (Wu *et al.*, 1996). El efecto TE se ha usado generalmente como escala para estudiar la estabilización de radicales debida a la deslocalización de spin, ya que tiene una correlación muy buena con los valores experimentales de las constantes de acoplamiento hiperfinas (hfc) de radicales bencílicos en ESR (Dust and Arnold, 1983). De la misma manera, los valores RSE isodésmicos para la serie de porfirinoides **3(a-h)** dio un buen coeficiente de correlación ($r = 0.940$) con los valores RSE para **6**. Sin embargo, los valores para las series de porfirinoides **4 β (a-h)** se desviaron de la esperada tendencia en los coeficientes de correlación ($r = 0.731$) y esta desviación es aún mayor para la serie de porfirinoides **4 α (a-h)** ($r = 0.660$). La diferencia en los números de onda ($\Delta\lambda$, nm) de la banda de absorción de mayor intensidad λ_{\max} para las porfirinas de la serie **3** [$\lambda(\mathbf{3}^{\cdot}) - \lambda(\mathbf{3})$] y para las de la serie **4** [$\lambda(\mathbf{4}^{\cdot}) - \lambda(\mathbf{4})$] dejó ver que los porfirinoides presentan efectos batocrómicos grandes (ca. 200 - 300 nm). www.relaquim.com

Palabras clave: porfirina, cálculos teóricos, radicales libres, efecto batocrómico.

INTRODUCTION

Free radicals (FR) are common species in biochemical processes, i.e. cellular respiration, homeostasis, autoimmune defense, and drugs metabolism (Pou *et al.*, 1998). Hemoglobine, which provides oxygen to tissue cells, and CYP enzymes, which catalyze the oxidation of organic substances, carry metal ions Fe(II) or Fe(III) domed in porphyrin rings acting as efficient redox-active centers (Meunier *et al.*, 2004).

Porphyrins electronic structure has been studied both experimentally and theoretically (Marsh and Mink, 1996; Shkirman *et al.*, 1999; Ali *et al.*, 2012). Absorption bands named α , β and γ (Soret band) appear in 650-550 nm, 530-500 nm, and 450-400 nm regions of UV-Vis spectra, respectively (Poole and Kalnenieks, 2000). The wavelength of maximal absorption (λ_{\max}) at the Soret band (also called B band) is essentially its pigmentary fingerprint (Lin *et al.*, 1994). The Soret absorption is strong and

generally associated with porphyrin-ring aromatic properties, which gives rise to a π - π^* electronic transition. Batho- and hypsochromic effects observed in α , β and γ bands as well as porphyrin fluorescence have been used a number of times in clinical studies to monitor drugs therapeutic effects and the presence of blood poisons and blood diseases (Poole and Kalnenieks, 2000; Reisch, 2012). Moreover, cancer treatments as photodynamic therapy (PDT) (Moan *et al.*, 1987) and boron neutron capture therapy (BNCT) (Barth *et al.*, 2005) rely on the selective delivery of porphyrins to tumors where they act as photosensitizers or energy carriers, respectively. Analogously, porphyrin pigments and radical congeners with ubiquitous molecular electronic properties (Ishida *et al.*, 2011) have inspired the production of new nano-scales optoelectronic materials.

Several years ago, the synthesis of porphyrin based prodrugs of general structure **1** (Figure 1) was initiated in my group (Ba-

ragán *et al.*, 2004; Barragán *et al.*, 2010) the ability of non cationic porphyrins to work as carriers of known antiviral drugs, as Azidovudine (AZT) which is in clinical use to treat HIV-1 infected people (Scruggs and Naylor, 2008), was investigated. The rationale behind prodrugs type-1 design is to increase bioavailability, selectivity, and drugs efficiency towards infected cells, thus diminishing side effects by reducing dosages as observed for other nucleotide prodrugs (Sofía *et al.*, 2012). Experiments using porphyrins electronic and fluorescence properties were performed observing that they indeed localize in the nucleus of infected B16 mouse melanoma line cells

in *in vitro* assays, thence highlighting their potential use as antitumor and antiviral carriers (Barragán *et al.*, 2005).

In this work, porphyrin series **2-5** (Figure 2) and FRs homolog series **3** and **4** (Figure 3) were calculated to furnish information on their structural geometry, relative stabilities, electronic properties and spin density (applicable only to FRs). A single aryl substituent was considered representative of the four meso substituents. Besides, one-substituent models aided to maintain a satisfactory CPU resources cost and time. The *p*-X-substituent at the phenyl ring was varied using atoms or groups that are able to directly interact with the

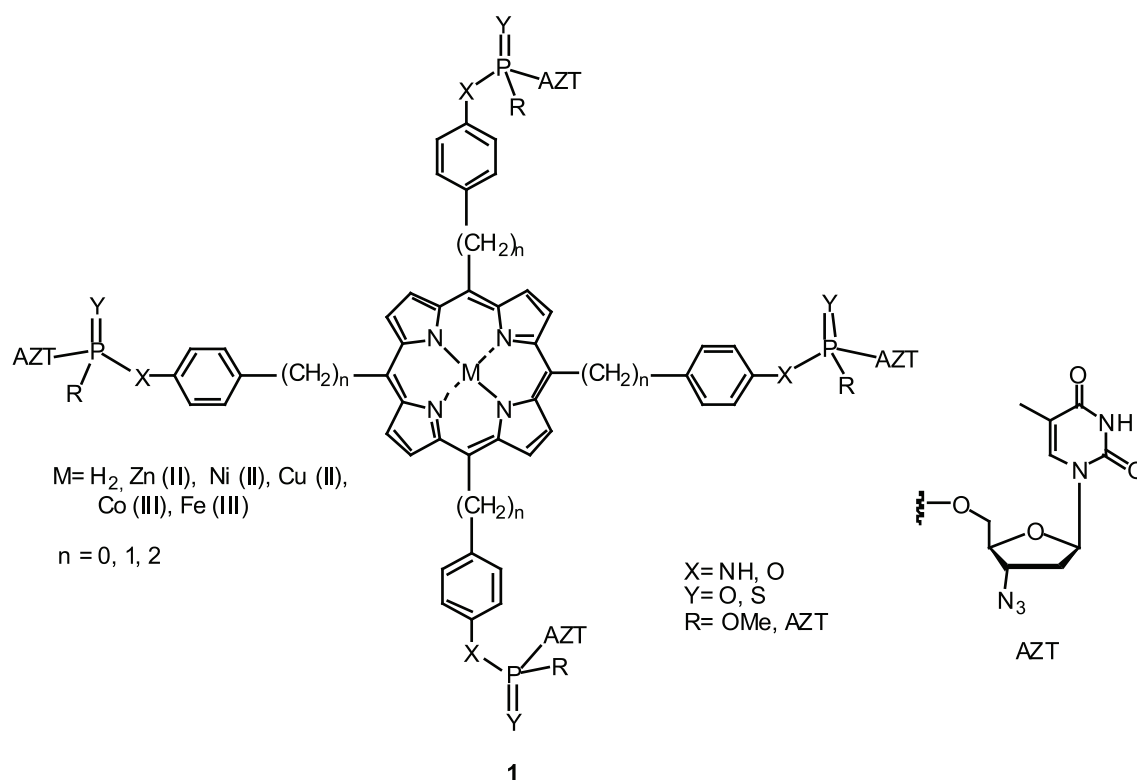


Figure 1. Porphyrinyl Prodrugs.

free radical center in FRs series **3** \cdot and **4** β \cdot increasing or decreasing its delocalization.

Porphyrinoid homolog series **3** \cdot and **4** \cdot are candidates to be active metabolites in prodrugs type-1 bioactivation processes, considering drug metabolism step catalyzed

by CYP119, a thermophilic P450 enzyme, that produces a C-H bond activation (Rittle and Green, 2010; Groves *et al.*, 1978) of the otherwise inactive C-H bond ($D \sim 100$ kcal/mol).

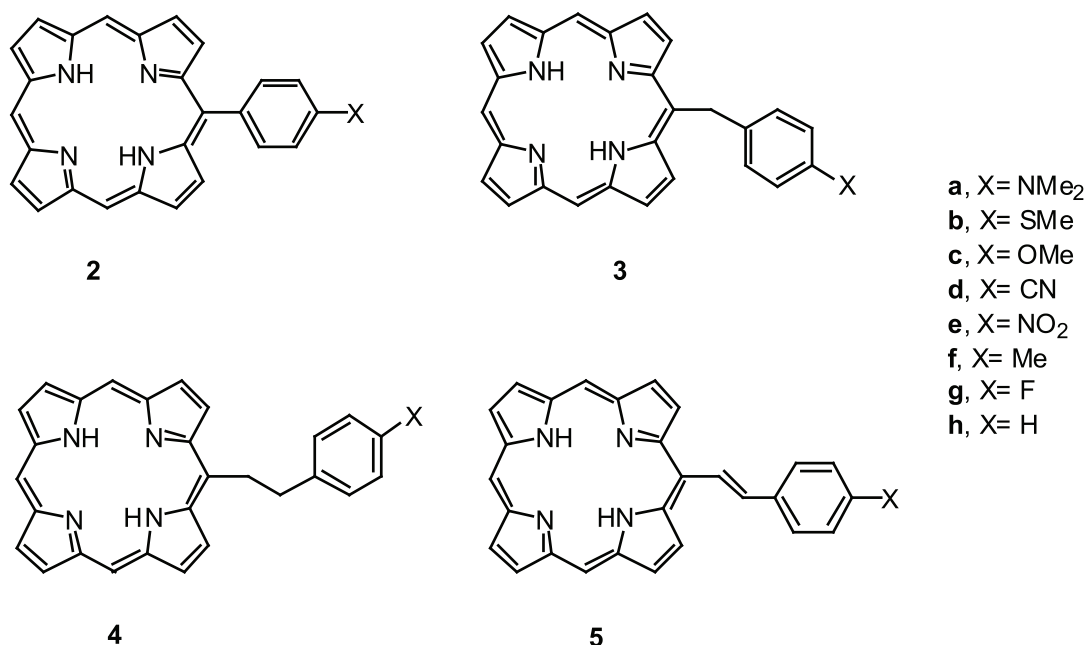


Figure 2. PP (**2a-2h**), BP (**3a-3h**), PeP (**4a-4h**) and CP (**5a-5h**) porphyrin series.

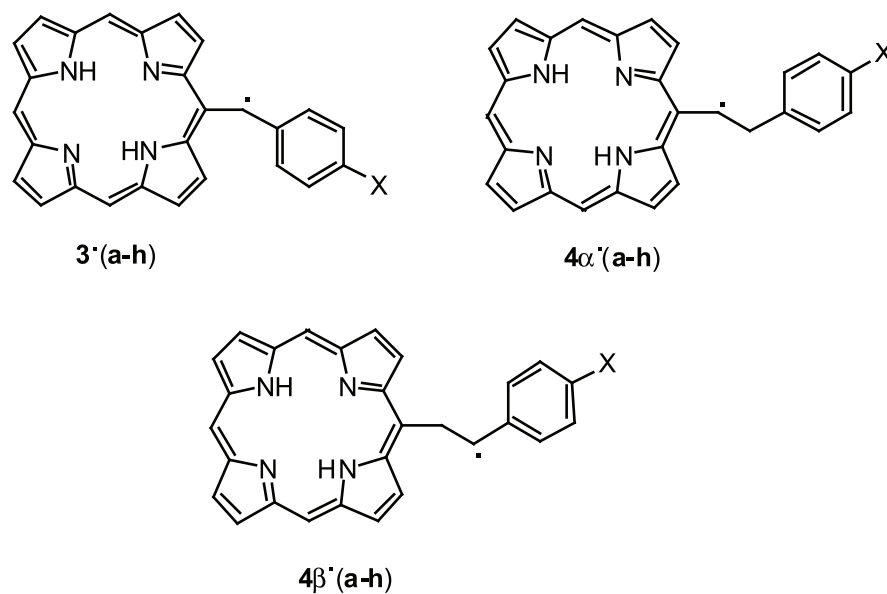


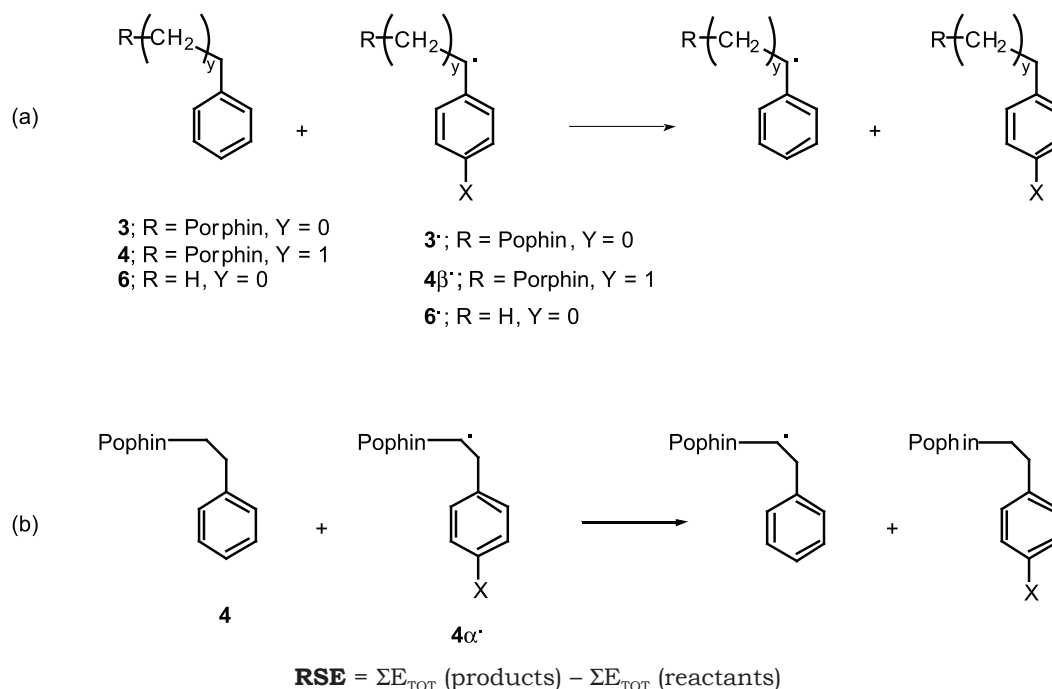
Figure 3. BP (**3**) and PeP (**4**) porphyrinoid series.

THEORETICAL CALCULATIONS

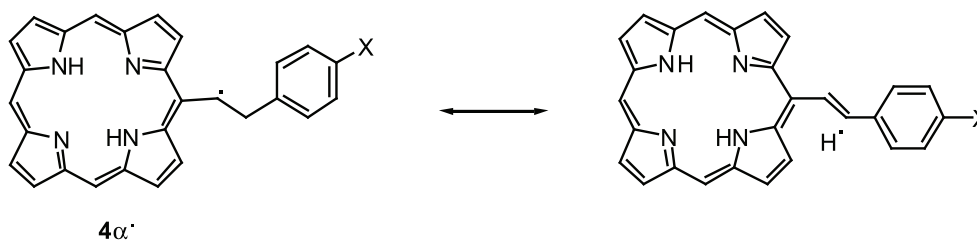
Geometry optimization of meso-(*p*-X-phenyl)porphin (PP) (**2a-2h**), meso-(*p*-X-benzyl)porphin (BP) (**3a-3h**), meso-(*p*-X-phenylethyl)porphin (PeP) (**4a-4h**), and meso-(*p*-X-cinnamyl)porphin (CP) (**5a-5h**) was performed by DFT using the B3LYP/6-31G(d,p) level of theory. An initial molecular mechanics conformational search employing the MMFF94 force field followed by frequency analysis of the equilibrium conformer using semiempirical AM1 calculations was practiced in each case. The corresponding open shell calculations of porphyrinyl radicaloids **3·** and **4·** were ca-

ried out using the spin-unrestricted B3LYP (UB3LYP) method and the 6-31G(d,p) basis set. All calculations were accomplished with Spartan'04 software package (Wavefunction, Irvine CA, USA). Neutral radical series BP (**3·**) and PeP (**4α·** and **4β·**) were generated individually at the radical center.

Optimized geometries and energies of porphyrinoids **3·** and **4·** were compared with their corresponding saturated porphyrins **3** and **4** through isodesmic reactions (Scheme 1) to gain insights on their stabilization origin. Radicaloid series PeP (**4·**) were also compared to CP (**5**) series in consideration to their stabilization by isovalent hyperconjugation, which is shown in Scheme 2 for **4α·**.



Scheme 1. Isodesmic reactions used to calculate radical stabilization energies (RSEs).



Scheme 2. Isovalent hyperconjugation in meso-(*p*-X-phenylethyl)porphin (PeP) (**4α·**) series.

Wavelength of maximal absorption (λ_{\max}) bands in UV-Vis spectra of the porphyrin **3** and **4** series were compared with the corresponding λ_{\max} of porphyrinoids **3** and **4** to examine the pigmentary fingerprints of porphyrin radicaloids by chromophoric λ_{\max} shifts. Since stable radicals (radical scavengers) are less toxic to normal cells than active short lived species, a study of the spin density at the radical center was carried out. Moreover, isodesmic radical stabilization energy (RSE) values of model benzyl radicals **6** (Scheme 1) were correlated with the FRs scales (σ_{C}) (Creary, 2006), (σ_{JJ}) (Jiang and Ji, 1992), and computational TE scale (Wu, *et al.*, 1996) to validate the theoretical method. RSE values of **3** and **4** were then linearly correlated with RSEs of **6** to glean information that helps

to improve the rational design of prodrugs type-**1** in redox active metabolic pathways and bioavailability.

RESULTS

Energy values of the optimized global minimum structure of each serial porphyrins **2-5** and FR series **3**, **4 α** , **4 β** are presented in Table 1 and 2 respectively. The calculated RSE values come from the isodesmic reactions shown in Scheme 1. The dihedral angles ω_1 , ω_2 and ω_3 which provide the relative orientation of the *p*-X-substituted phenyl ring respect to the porphin ring are defined in Figure 4 and listed in Table 3 for porphyrins series **2-5** and in Table 4 for porphyrinoids **3** and **4** series.

Table 1. Total energy (au) of the *p*-X-substituted porphyrins **2(a-h)** - **5(a-h)**.

X	2	3	4	5
a , NMe ₂	-1354.60827	-1393.92004	-1433.23842	-1432.01616
b , SMe	-1658.13871	-1697.45008	-1736.76882	-1735.54520
c , OMe	-1335.15980	-1374.47196	-1413.79019	-1412.56674
d , CN	-1312.87592	-1352.18968	-1391.50774	-1390.28334
e , NO ₂	-1425.13425	-1464.44830	-1503.76631	-1502.54207
f , Me	-1259.95524	-1299.26770	-1338.58603	-1337.36198
g , F	-1319.86615	-1359.17879	-1398.49704	-1397.27271
h , H	-1220.63449	-1259.94710	-1299.26546	-1298.04106

Table 2. Total energy (au) of the *p*-X-substituted porphyrinoids **3(a-h)**, **4 α (a-h)**, **4 β (a-h)** and calculated radical stabilization energy (RSE)^a values in kcal/mol.

X	E _{TOT} 3	RSE 3	E _{TOT} 4α	RSE 4α	E _{TOT} 4β	RSE 4β
a , NMe ₂	-1393.28844	2.25	-1432.59821	1.26	-1432.59168	1.29
b , SMe	-1696.81664	1.10	-1736.12676	0.10	-1736.12146	0.90
c , OMe	-1373.83816	0.87	-1413.14989	1.20	-1413.14222	0.51
d , CN	-1351.55464	0.09	-1390.86700	0.93	-1390.86077	1.14
e , NO ₂	-1463.81359	0.30	-1503.12398	-0.07	-1503.11974	1.39
f , Me	-1298.63299	0.30	-1337.94388	0.04	-1337.93763	0.24
g , F	-1358.54378	0.11	-1397.85485	0.02	-1397.84831	0.04
h , H	-1259.31191	0.00	-1298.62324	0.00	-1298.61667	0.00

^a Positive RSE values indicate *p*-X-substituted porphyrinoids are more stable than the parent (X = H) porphyrinoid.

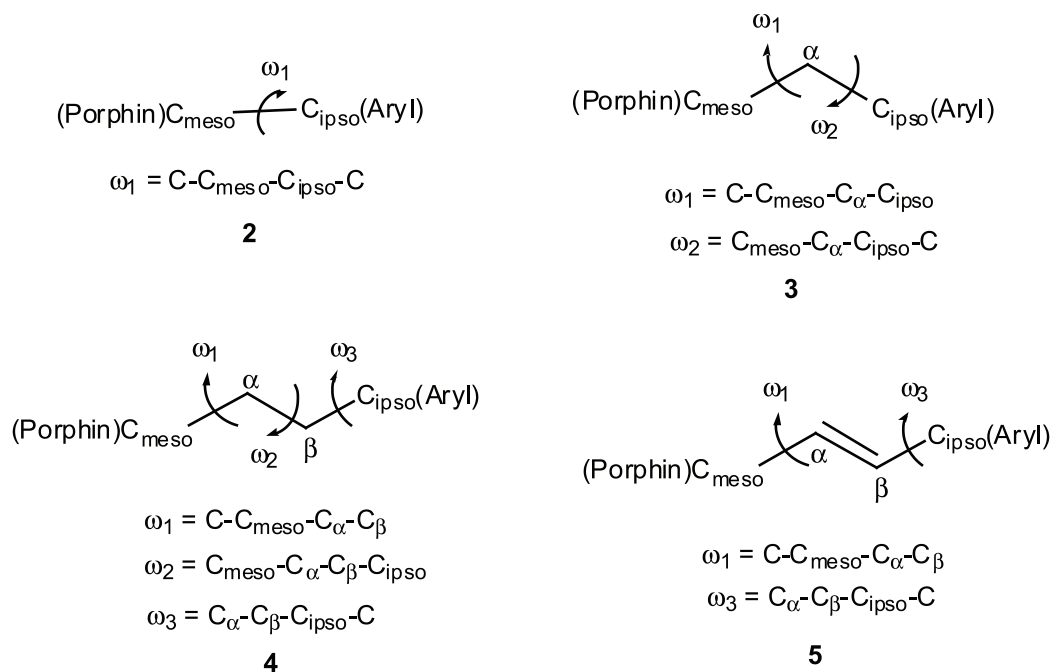


Figure 4. Dihedral angle ω_1 , ω_2 and ω_3 definitions for porphyrin **2-5** and porphyrinoid **3** and **4** structures.

Table 3. Torsion angles ω_1 , ω_2 , and ω_3 for porphyrin **2(a-h)** - **5(a-h)**.^a

X	2	3	4	5
a , NMe ₂	$\omega_1 = -90^\circ$	$\omega_1 = 78^\circ$ $\omega_2 = 43^\circ$	$\omega_1 = -90^\circ$ $\omega_2 = -179^\circ$ $\omega_3 = -87^\circ$	$\omega_1 = -41^\circ$ $\omega_3 = -10^\circ$
b , SMe	$\omega_1 = -65^\circ$	$\omega_1 = 79^\circ$ $\omega_2 = 35^\circ$	$\omega_1 = -92^\circ$ $\omega_2 = -180^\circ$ $\omega_3 = -88^\circ$	$\omega_1 = -41^\circ$ $\omega_3 = -10^\circ$
c , OMe	$\omega_1 = -90^\circ$	$\omega_1 = 78^\circ$ $\omega_2 = 40^\circ$	$\omega_1 = -92^\circ$ $\omega_2 = -179^\circ$ $\omega_3 = -89^\circ$	$\omega_1 = 42^\circ$ $\omega_3 = 7^\circ$
d , CN	$\omega_1 = -90^\circ$	$\omega_1 = 79^\circ$ $\omega_2 = 28^\circ$	$\omega_1 = -91^\circ$ $\omega_2 = -179^\circ$ $\omega_3 = -87^\circ$	$\omega_1 = -40^\circ$ $\omega_3 = -12^\circ$
e , NO ₂	$\omega_1 = -90^\circ$	$\omega_1 = 77^\circ$ $\omega_2 = 35^\circ$	$\omega_1 = -91^\circ$ $\omega_2 = -180^\circ$ $\omega_3 = -87^\circ$	$\omega_1 = -42^\circ$ $\omega_3 = -17^\circ$
f , Me	$\omega_1 = -90^\circ$	$\omega_1 = 78^\circ$ $\omega_2 = 33^\circ$	$\omega_1 = -91^\circ$ $\omega_2 = -180^\circ$ $\omega_3 = -88^\circ$	$\omega_1 = -44^\circ$ $\omega_3 = -16^\circ$
g , F	$\omega_1 = -90^\circ$	$\omega_1 = 77^\circ$ $\omega_2 = 34^\circ$	$\omega_1 = -91^\circ$ $\omega_2 = -180^\circ$ $\omega_3 = -88^\circ$	$\omega_1 = 44^\circ$ $\omega_3 = 16^\circ$
h , H	$\omega_1 = -90^\circ$	$\omega_1 = 77^\circ$ $\omega_2 = 34^\circ$	$\omega_1 = -91^\circ$ $\omega_2 = -180^\circ$ $\omega_3 = -88^\circ$	$\omega_1 = 44^\circ$ $\omega_3 = 16^\circ$

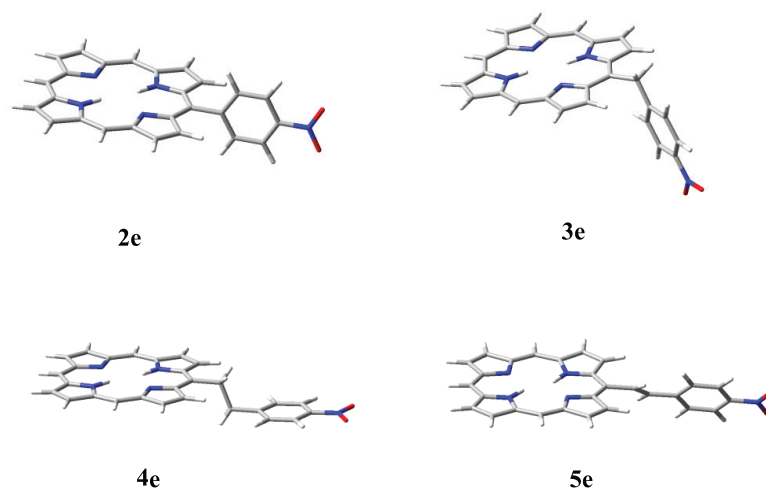
^a Torsion angle definitions in Fig. 4.

Table 4. Torsion angles ω_1 , ω_2 , and ω_3 for porphyrinoids **3(a-h)**, **4 α (a-h)**, **4 β (a-h)**.^a

X	3 [•]	4α [•]	4β [•]
a , NMe ₂	$\omega_1 = -19^\circ$ $\omega_2 = -25^\circ$	$\omega_1 = -6^\circ$ $\omega_2 = -149^\circ$ $\omega_3 = 63^\circ$	$\omega_1 = -83^\circ$ $\omega_2 = 166^\circ$ $\omega_3 = 1^\circ$
b , SMe	$\omega_1 = -19^\circ$ $\omega_2 = -29^\circ$	$\omega_1 = 5^\circ$ $\omega_2 = -115^\circ$ $\omega_3 = 38^\circ$	$\omega_1 = -83^\circ$ $\omega_2 = 164^\circ$ $\omega_3 = 1^\circ$
c , OMe	$\omega_1 = -17^\circ$ $\omega_2 = -28^\circ$	$\omega_1 = -5^\circ$ $\omega_2 = -147^\circ$ $\omega_3 = 69^\circ$	$\omega_1 = -84^\circ$ $\omega_2 = 168^\circ$ $\omega_3 = 1^\circ$
d , CN	$\omega_1 = -20^\circ$ $\omega_2 = -29^\circ$	$\omega_1 = -5^\circ$ $\omega_2 = -147^\circ$ $\omega_3 = -65^\circ$	$\omega_1 = -80^\circ$ $\omega_2 = 164^\circ$ $\omega_3 = 1^\circ$
e , NO ₂	$\omega_1 = 22^\circ$ $\omega_2 = 27^\circ$	$\omega_1 = 6^\circ$ $\omega_2 = -113^\circ$ $\omega_3 = 30^\circ$	$\omega_1 = -82^\circ$ $\omega_2 = 164^\circ$ $\omega_3 = 0^\circ$
f , Me	$\omega_1 = 17^\circ$ $\omega_2 = 31^\circ$	$\omega_1 = 5^\circ$ $\omega_2 = -114^\circ$ $\omega_3 = 36^\circ$	$\omega_1 = -83^\circ$ $\omega_2 = 168^\circ$ $\omega_3 = 1^\circ$
g , F	$\omega_1 = 16^\circ$ $\omega_2 = 33^\circ$	$\omega_1 = 5^\circ$ $\omega_2 = -115^\circ$ $\omega_3 = 35^\circ$	$\omega_1 = 84^\circ$ $\omega_2 = -170^\circ$ $\omega_3 = 0^\circ$
h , H	$\omega_1 = 17^\circ$ $\omega_2 = 33^\circ$	$\omega_1 = 5^\circ$ $\omega_2 = -116^\circ$ $\omega_3 = 37^\circ$	$\omega_1 = -84^\circ$ $\omega_2 = 168^\circ$ $\omega_3 = 0^\circ$

^a Torsion angle definitions in Fig. 4.

The optimized porphyrin structures **2e-5e** and FR porphyrins **3e** and **4e** are shown in Figure 5 and Figure 6, respectively.

**Figure 5.** Optimized porphyrin **2e-5e** structures at the B3LYP/6-31G(d,p) level of theory.

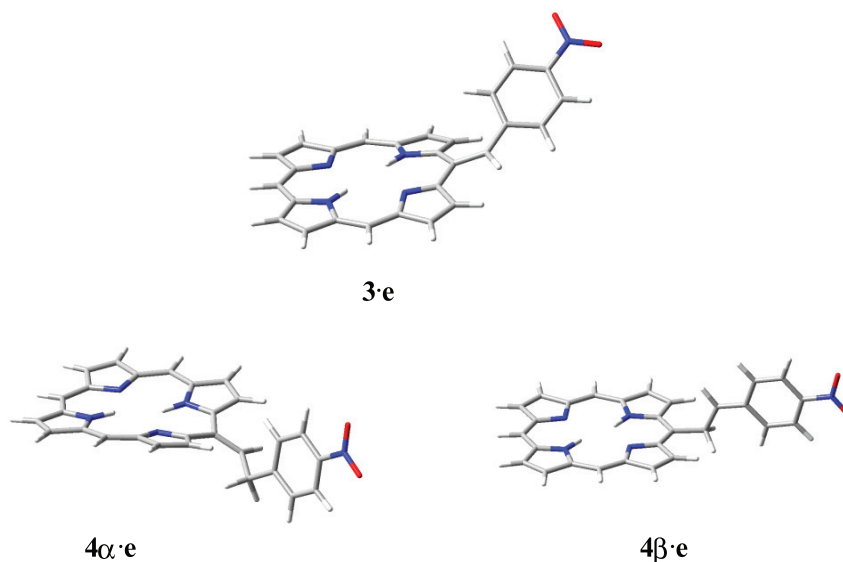


Figure 6. Optimized porphyrinoid **3·e**, **4 α ·e**, and **4 β ·e** structures at the UB3LYP/6-31G(d,p) level of theory.

DFT calculated UV-Vis spectra of serial porphyrins **2-5** and porphyrinoids **3** and **4** at the B3LYP/6-31G(d,p) and at the UB3LYP/6-31G(d,p) levels of theory, respectively, displayed a wavelength of maximal absorption (λ_{\max}) in the Soret band region (around 400 nm) for the parent por-

phyrins (Table 5) and at longer wavelengths region (Table 6) for the corresponding radicals. The red shift (bathochromic effect) in the λ_{\max} of porphyrinoids is quantitated by the difference maximal absorption wavelength $\Delta\lambda_{\max} = [\lambda_{\max}(\text{porphyrinoid}) - \lambda_{\max}(\text{porphyrin})]$, which is included in Table 6.

Table 5. Wavelengths of maximal absorption (λ_{\max}) for porphyrins **2(a-h)** - **5(a-h)**.

X	λ_{\max} 2	λ_{\max} 3	λ_{\max} 4	λ_{\max} 5
a , NMe ₂	360	^a 362	485	^b 457
b , SMe	399	362	410	424
c , OMe	360	390	386	408
d , CN	354	357	356	400
e , NO ₂	361	434	474	^c 462
f , Me	353	357	353	384
g , F	354	357	353	377
h , H	353	355	353	375

^a A second intense band appears at 489 nm. ^b A second intense band appears at 371 nm. ^c A second intense band appears at 535 nm.

Table 6. Wavelengths of maximal absorption (λ_{\max}) for porphyrinoids **3**·(a-h) **4**·(a-h) and relative $\Delta\lambda_{\max}$ = [λ_{\max} (porphyrinoid) - λ_{\max} (porphyrin)].

X	λ_{\max} 3 ·	$\Delta\lambda_{\max}$ [3 ·- 3]	λ_{\max} 4 ·	$\Delta\lambda_{\max}$ [4 ·- 4]	λ_{\max} 4 β·	$\Delta\lambda_{\max}$ [4 β·- 4]
a , NMe ₂	561	199	650	165	858	373
b , SMe	558	159	661	251	685	275
c , OMe	555	195	653	267	712	326
d , CN	553	199	654	298	627	271
e , NO ₂	^a 596	162	661	187	654	180
f , Me	545	192	660	307	655	302
g , F	541	187	660	307	627	274
h , H	541	188	660	307	624	271

^a A second intense band appears at 567 nm.

DISCUSSION

Theoretical Method Validation

In order to validate the isodesmic method employed to study the stabilization energy of porphyrinoid **3**· and **4**· series, radical stabilization energy (RSE) values for model *p*-X-substituted benzyl radicals **6**·(a-h) (Scheme 1) were calculated with DFT at the UB3LYP/6-31G(d,p) level of theory following the same procedure described above for **3**· and **4**·. The RSE values for **6**· series are compiled in Table 7. RSE values were then related to the computational

radical total effect (TE) values obtained by DFT at the level BLYP/6-31G(d) (Wu, *et al.*, 1996) (Table 7). As observed, RSE values are smaller than TE values, however a plot of RSE against TE gave a linear regression (slope = 0.789) with quite good correlation (*r* = 0.989).

TE values are generally accepted as a scale to measure substituent effects in free radicals stabilization that depend on spin delocalization more than on polar effects. Wu scale correlation with measured ESR hyperfine coupling constants (hfc) of benzyl radicals (Dust and Arnold, 1983), at the

Table 7. Total energy (au) of the *p*-X-substituted benzyl radicals **6**·(a-h), calculated radical stabilization energy (RSE) values in kcal/mol and TE scale values in kcal/mol.

X	E _{TOT} 6	E _{TOT} 6 ·	^a RSE	^b TE scale
a , NMe ₂	-405.551158	-404.901296	1.75	2.19
b , SMe	-709.082180	-708.431159	1.02	1.40
c , OMe	-386.103373	-385.451923	0.76	1.08
d , CN	-363.821634	-363.169956	0.61	0.86
e , NO ₂	-476.080210	-475.428504	0.59	1.04
f , Me	-310.899238	-310.247163	0.36	0.42
g , F	-370.810435	-370.157826	0.03	0.16
h , H	-271.578818	-270.926164	0.00	0.00

^a Positive RSE values indicate *p*-X-substituted benzyl radicals are more stable than the parent (X = H) benzyl radical. ^b Wu, *et al.*, 1996.

radical center, is fairly good. RSE values for **6(a-h)** series were also plotted against FRs scales (σ_{C}) (Creary, 2006) and (σ_{JJ}) (Jiang and Ji, 1992) providing good correlations (0.911 and 0.969, respectively). These results confirm the validity of the isodesmic model and calculations level of theory used here to simulate neutral free radicals.

Benzyl radicals **6** are delocalized, thus radical centers tend to be planar. Table 8 collects the interplanar angles $\zeta_1 - \zeta_3$ that define the planarity of the radical center according to the planes $\sigma_1 - \sigma_3$ defined in Figure 7. Consequently, a completely planar radical must display $\zeta_1 = \zeta_2 = \zeta_3 = 0$.

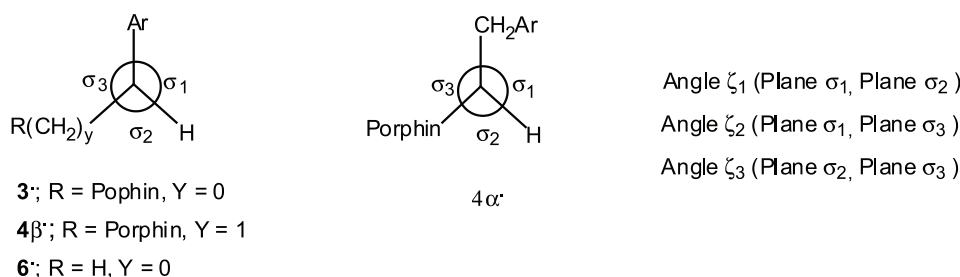


Figure 7. Interplanar angle ζ_1 , ζ_2 and ζ_3 definitions for **3**, **4 α** , **4 β** and **6** structures.

Table 8. Interplanar angles ζ_1 , ζ_2 and ζ_3 of *p*-X-substituted benzyl radicals **6(a-h)**, spin density (SD) values at C_{para} (C_{p}), and SD ratios [$R_{\text{SD}} = \text{SD}(C_{\alpha})/\text{SD}(C_{\text{p}})$].

X	6	SD	^a SD
a , NMe ₂	$\zeta_1 = 4.7^\circ$	$C_{\alpha} = 0.682$	$C_{\alpha} = 0.589$
	$\zeta_2 = 3.9^\circ$	$C_{\text{p}} = 0.173$	$C_{\text{p}} = 0.157$
	$\zeta_3 = 4.8^\circ$	$R_{\text{SD}} = 3.94$	$R_{\text{SD}} = 3.75$
b , SMe	$\zeta_1 = 4.7^\circ$	$C_{\alpha} = 0.692$	$C_{\alpha} = 0.598$
	$\zeta_2 = 3.9^\circ$	$C_{\text{p}} = 0.220$	$C_{\text{p}} = 0.196$
	$\zeta_3 = 4.8^\circ$	$R_{\text{SD}} = 3.15$	$R_{\text{SD}} = 3.05$
c , OMe	$\zeta_1 = 4.4^\circ$	$C_{\alpha} = 0.708$	$C_{\alpha} = 0.617$
	$\zeta_2 = 3.6^\circ$	$C_{\text{p}} = 0.198$	$C_{\text{p}} = 0.178$
	$\zeta_3 = 4.5^\circ$	$R_{\text{SD}} = 3.58$	$R_{\text{SD}} = 3.47$
d , CN	$\zeta_1 = 4.9^\circ$	$C_{\alpha} = 0.688$	$C_{\alpha} = 0.595$
	$\zeta_2 = 4.1^\circ$	$C_{\text{p}} = 0.230$	$C_{\text{p}} = 0.206$
	$\zeta_3 = 5.1^\circ$	$R_{\text{SD}} = 2.99$	$R_{\text{SD}} = 2.89$
e , NO ₂	$\zeta_1 = 4.1^\circ$	$C_{\alpha} = 0.684$	$C_{\alpha} = 0.584$
	$\zeta_2 = 5.0^\circ$	$C_{\text{p}} = 0.212$	$C_{\text{p}} = 0.190$
	$\zeta_3 = 5.1^\circ$	$R_{\text{SD}} = 3.23$	$R_{\text{SD}} = 3.07$
f , Me	$\zeta_1 = 3.5^\circ$	$C_{\alpha} = 0.716$	$C_{\alpha} = 0.630$
	$\zeta_2 = 4.2^\circ$	$C_{\text{p}} = 0.239$	$C_{\text{p}} = 0.218$
	$\zeta_3 = 4.3^\circ$	$R_{\text{SD}} = 2.99$	$R_{\text{SD}} = 2.89$
g , F	$\zeta_1 = 3.5^\circ$	$C_{\alpha} = 0.724$	$C_{\alpha} = 0.636$
	$\zeta_2 = 4.2^\circ$	$C_{\text{p}} = 0.210$	$C_{\text{p}} = 0.195$
	$\zeta_3 = 4.4^\circ$	$R_{\text{SD}} = 3.45$	$R_{\text{SD}} = 3.26$
h , H	$\zeta_1 = 4.4^\circ$	$C_{\alpha} = 0.725$	$C_{\alpha} = 0.640$
	$\zeta_2 = 3.7^\circ$	$C_{\text{p}} = 0.243$	$C_{\text{p}} = 0.215$
	$\zeta_3 = 4.5^\circ$	$R_{\text{SD}} = 2.98$	$R_{\text{SD}} = 2.98$

^a Wu, *et al.*, 1996

Interplanar angles for **6**· series are close to zero (3.5° - 5.1°). The slight deviation from planarity do not depend on X substitution. In accord with the expected ring spin delocalization (SD), spin density at the radical center (C_o) is three to four times the spin density at the *para* position (C_p) of the phenyl ring [$R_{SD} = SD(C_o)/SD(C_p)$] (Table 8). Taking into consideration the SD value for C_o (0.725) of the parent benzyl radical (X = H), electron donating (X = NMe₂, SMe) and electron withdrawing (X = CN, NO₂) groups in substituted benzyl radicals promote spin delocalization more than the other groups (X = OMe, Me, F). A highly precise correlation of SDs of this work vs. Wu values (Table 8) was found ($r = 0.994$).

Stabilization and geometry of porphyrinoid **3**·(a-h) and **4**·(a-h) series

The isodesmic RSE values for porphyrinoid **3**·(a-h) and **4**·(a-h) series are summarized in Table 2. Both electron donating and withdrawing groups stabilize radical **3**· and **4**β· series but the effect is lost in **4**α· series. The methine radical center in porphyrinoid **3**· series is acting as a linkage topological group of two independent aromatic moieties, the porphin and the *p*-X-substituted phenyl rings. Even though these two rings are not coplanar in **3**· (dihedral angles ω_1 and ω_2 are between 16° - 22° and between 25° - 33°, respectively, as observed in Table 4 and in structure **3**·e of Figure 6), RSE values are, in general, higher than RSEs of benzyl radicals **6**· (Table 7), thus indicating that stabilization due to X substituents in the methine radical center of **3**· is afforded more efficiently than in the methylene radical center of **6**·. This is certainly not the case for the methine radical center of **4**β· where the porphin ring is not directly linked to the radical center but through a methylene group. RSEs of **4**β· are, in general, smaller than RSEs of **6**·. A plot of RSE values of **3**· against RSE values of **6**· gives a linear correlation with slope of 1.26 and $r = 0.940$.

Meanwhile, the plot of RSEs values of **4**β· vs. RSEs of **6**· gives a poor correlation ($r = 0.731$); however, this plot gives an excellent correlation ($r = 0.991$) if two points, belonging to the X groups NO₂ and CN, which are scattered, are not taken into account in the linear regression (slope = 0.757). For **4**α· porphyrinoid series a direct influence of the *p*-X-substituents on the methine radical center is not expected since the radical center is separated from the aryl ring by a methylene group, however RSE values were calculated in consideration to the possible radical stabilization by isovalent hyperconjugation (Scheme 2). RSEs of **4**α· were then plotted against RSEs of **6**· observing a poor correspondence between the two data sets ($r = 0.660$) with scattering of the points. Regarding geometry of radicaloids **4**α· and **4**β· none of them presented the porphin and aryl rings in a coplanar arrangement (see dihedral angles ω_1 - ω_3 in Table 4 and structures **4**α·e and **4**β·e in Figure 6), although saturated porphyrins **4** series do (see for example structure **4**e in Figure 5).

The extent of planarity at the methine radical center of **3**·, **4**α· and **4**β· was investigated through the interplanar angles ζ_1 - ζ_3 , whose definitions follow structures in Figure 7. These angles are collected in Table 9. Meanwhile slight deviations of planarity are observed for **3**· (3.5° - 5.1°) and **4**α· (3.3° - 5.3°) series, as those reported for **6**· series (see above), practically planar radicals are observed in the case of **4**β· (0.3° - 1.5°) series. As pointed out by Wu (Wu, 1996), relative radical stabilities of **6**· series are mainly determined by spin delocalization more than by polar effects, thus increasing planarity of the radical center in **4**β· is expected to favor spin delocalization.

Table 9. Interplanar angles $\zeta_1 - \zeta_3$ and spin density (SD) at various positions (see Scheme 3) for porphyrinoids **3**·(a-h), **4**α· (a-h) and **4**β· (a-h). Interplanar angle ζ_4 for **3**·(a-h) series (see Fig. 8).

X	3 ·	SD 3 ·	4 α·	SD 4 α·	4 β·	SD 4 β·
NMe ₂	$\zeta_1 = 4.7^\circ$	$C_\alpha = 0.296$	$\zeta_1 = 3.8^\circ$	$C_\alpha = 0.282$	$\zeta_1 = 0.6^\circ$	$C_\beta = 0.651$
	$\zeta_2 = 3.9^\circ$	$C_p = 0.058$	$\zeta_2 = 4.4^\circ$	$C_p = -0.001$	$\zeta_2 = 0.7^\circ$	$C_p = 0.163$
	$\zeta_3 = 4.8^\circ$	$C_{m2} = 0.216$	$\zeta_3 = 4.5^\circ$	$C_{m2} = 0.253$	$\zeta_3 = 0.7^\circ$	$C_{m2} = -0.003$
	$\zeta_4 = 35.0^\circ$					
SMe	$\zeta_1 = 4.7^\circ$	$C_\alpha = 0.321$	$\zeta_1 = 3.7^\circ$	$C_\alpha = 0.260$	$\zeta_1 = 0.3^\circ$	$C_\beta = 0.660$
	$\zeta_2 = 3.9^\circ$	$C_p = 0.073$	$\zeta_2 = 4.2^\circ$	$C_p = 0.002$	$\zeta_2 = 0.4^\circ$	$C_p = 0.205$
	$\zeta_3 = 4.8^\circ$	$C_{m2} = 0.216$	$\zeta_3 = 4.3^\circ$	$C_{m2} = 0.256$	$\zeta_3 = 0.4^\circ$	$C_{m2} = -0.003$
	$\zeta_4 = 37.9^\circ$					
OMe	$\zeta_1 = 4.4^\circ$	$C_\alpha = 0.319$	$\zeta_1 = 3.5^\circ$	$C_\alpha = 0.280$	$\zeta_1 = 0.7^\circ$	$C_\beta = 0.676$
	$\zeta_2 = 3.6^\circ$	$C_p = 0.066$	$\zeta_2 = 4.0^\circ$	$C_p = 0.001$	$\zeta_2 = 0.8^\circ$	$C_p = 0.183$
	$\zeta_3 = 4.5^\circ$	$C_{m2} = 0.216$	$\zeta_3 = 4.1^\circ$	$C_{m2} = 0.254$	$\zeta_3 = 0.7^\circ$	$C_{m2} = -0.003$
	$\zeta_4 = 35.9^\circ$					
CN	$\zeta_1 = 4.9^\circ$	$C_\alpha = 0.329$	$\zeta_1 = 3.3^\circ$	$C_\alpha = 0.273$	$\zeta_1 = 0.9^\circ$	$C_\beta = 0.650$
	$\zeta_2 = 4.1^\circ$	$C_p = 0.081$	$\zeta_2 = 3.7^\circ$	$C_p = -0.001$	$\zeta_2 = 1.0^\circ$	$C_p = 0.214$
	$\zeta_3 = 5.1^\circ$	$C_{m2} = 0.212$	$\zeta_3 = 3.8^\circ$	$C_{m2} = 0.255$	$\zeta_3 = 1.0^\circ$	$C_{m2} = -0.002$
	$\zeta_4 = 38.5^\circ$					
NO ₂	$\zeta_1 = 4.1^\circ$	$C_\alpha = 0.339$	$\zeta_1 = 4.5^\circ$	$C_\alpha = 0.262$	$\zeta_1 = 1.2^\circ$	$C_\beta = 0.639$
	$\zeta_2 = 5.0^\circ$	$C_p = 0.082$	$\zeta_2 = 5.1^\circ$	$C_p = 0.002$	$\zeta_2 = 1.3^\circ$	$C_p = 0.197$
	$\zeta_3 = 5.1^\circ$	$C_{m2} = 0.201$	$\zeta_3 = 5.3^\circ$	$C_{m2} = 0.256$	$\zeta_3 = 1.3^\circ$	$C_{m2} = -0.002$
	$\zeta_4 = 38.5^\circ$					
Me	$\zeta_1 = 3.7^\circ$	$C_\alpha = 0.313$	$\zeta_1 = 3.8^\circ$	$C_\alpha = 0.262$	$\zeta_1 = 0.7^\circ$	$C_\beta = 0.683$
	$\zeta_2 = 4.5^\circ$	$C_p = 0.071$	$\zeta_2 = 4.4^\circ$	$C_p = 0.002$	$\zeta_2 = 0.8^\circ$	$C_p = 0.220$
	$\zeta_3 = 4.6^\circ$	$C_{m2} = 0.223$	$\zeta_3 = 4.5^\circ$	$C_{m2} = 0.256$	$\zeta_3 = 0.8^\circ$	$C_{m2} = -0.003$
	$\zeta_4 = 37.1^\circ$					
F	$\zeta_1 = 3.5^\circ$	$C_\alpha = 0.308$	$\zeta_1 = 4.0^\circ$	$C_\alpha = 0.261$	$\zeta_1 = 1.1^\circ$	$C_\beta = 0.691$
	$\zeta_2 = 4.2^\circ$	$C_p = 0.059$	$\zeta_2 = 4.7^\circ$	$C_p = 0.002$	$\zeta_2 = 1.2^\circ$	$C_p = 0.193$
	$\zeta_3 = 4.4^\circ$	$C_{m2} = 0.226$	$\zeta_3 = 4.8^\circ$	$C_{m2} = 0.256$	$\zeta_3 = 1.2^\circ$	$C_{m2} = -0.003$
	$\zeta_4 = 39.0^\circ$					
H	$\zeta_1 = 4.4^\circ$	$C_\alpha = 0.312$	$\zeta_1 = 4.1^\circ$	$C_\alpha = 0.260$	$\zeta_1 = 1.4^\circ$	$C_\beta = 0.690$
	$\zeta_2 = 3.7^\circ$	$C_p = 0.068$	$\zeta_2 = 4.8^\circ$	$C_p = 0.002$	$\zeta_2 = 1.5^\circ$	$C_p = 0.223$
	$\zeta_3 = 4.5^\circ$	$C_{m2} = 0.226$	$\zeta_3 = 4.9^\circ$	$C_{m2} = 0.256$	$\zeta_3 = 1.5^\circ$	$C_{m2} = -0.003$
	$\zeta_4 = 39.7^\circ$					

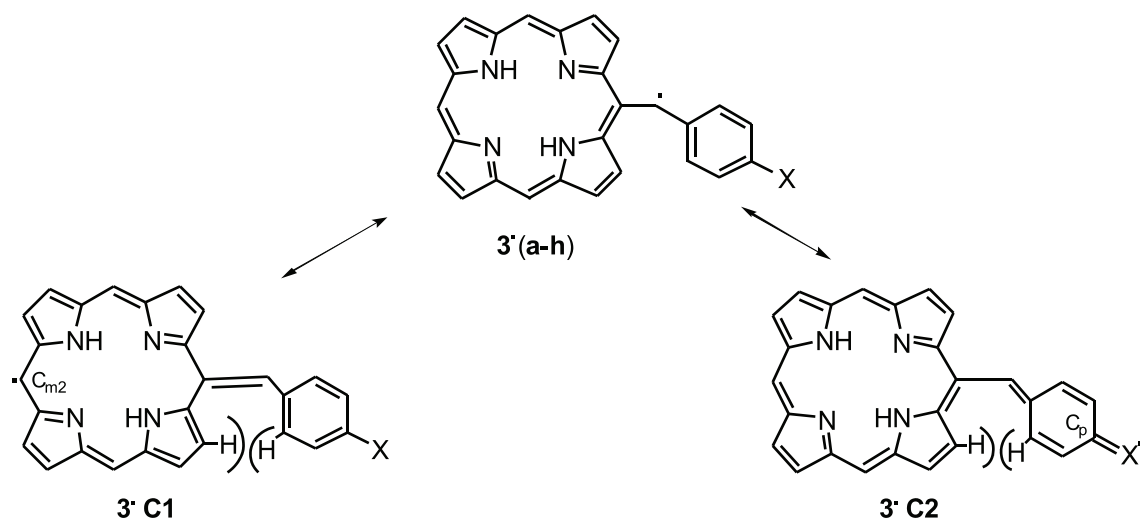
Indeed, spin density (SD) at the C_β radical center of porphyrinoid **4**β· series (Table 9) are smaller than those at the C_α radical center of **6**· series (SDs of this work in Table 8), indicating an increase of radical delocalization for the first series. The tendency in spin delocalization for **4**β· series is $\text{NO}_2 > \text{CN} > \text{NMe}_2 > \text{SMe} > \text{OMe} > \text{Me} > \text{H} > \text{F}$, meanwhile for **6**· series is

$\text{NMe}_2 > \text{NO}_2 > \text{CN} > \text{SMe} > \text{OMe} > \text{Me} > \text{F} > \text{H}$.

With respect to **3**· series, SD values at the C_α radical center (summarized in Table 9) are considerably smaller than SD values at the C_β radical center of **4**β· series confirming spin delocalization through the porphyrin ring in **3**· series, which is neglected in the case of **4**β· series. As indicated above, the two aromatic rings in porphyrinoids **3**·

are not coplanar, steric hindrance between peripheral hydrogens keeps geometry of canonical forms $\mathbf{3}\cdot\text{C1}$ and $\mathbf{3}\cdot\text{C2}$ from attain planarity (Scheme 3). The angle between the pophin and aryl rings (ζ_4) in $\mathbf{3}\cdot$ series varies between 35.0° and 39.7° (Table 9), ζ_4 is defined in Figure 8.

The noncoplanarity of these aromatic rings prevents radicaloids $\mathbf{3}\cdot$ from being highly delocalized as a whole, however spin delocalization is indeed observed in both rings. This is, SD values at the meso2 position (C_{m2}) of $\mathbf{3}\cdot$ series are sizable (0.201 to 0.226) as compared with SD vales of



Scheme 3. Structures in resonance in porphyrinoid $\mathbf{3}\cdot$ series.

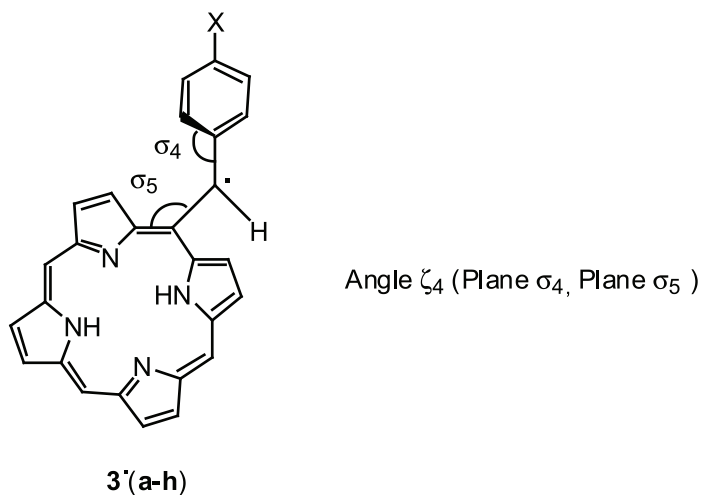


Figure 8. Interplanar angle ζ_4 definition for $\mathbf{3}\cdot$ structures.

4 β series (-0.002 to -0.003) (Table 9), SD values at C_p position of **3** series are small (0.058 to 0.082) but larger than those of **4 α** series (-0.001 to 0.002) in which spin delocalization through the aryl ring is not possible unless the participation of isovalent hyperconjugation (Scheme 2) is important.

Uv-Vis spectra calculations for porphyrins 2-5 and porphyrinoids 3, 4 series

Measured wavelengths of the maximal absorption band (λ_{\max}) of porphin (372.5 nm, vapor) and tetraphenylporphyrin (402.5 nm, vapor) are related to their Soret bands (Edwards *et al.*, 1971). Calculated absorption spectra of porphin and tetraphenylporphyrin at the B3LYP/6-31G(d,p) level of theory displayed λ_{\max} absorption bands at 351 nm and at 367 nm, respectively. Thus, it seems reasonable to assume that calculated Soret bands reported here are shifted to shorter wavelengths by around 20 - 35 nm compared to the experimental wavelengths. Absorption spectra of serial porphyrins **2-5** and porphyrinoids **3**, **4** are compiled in Tables 5 and 6, respectively. The porphin and the *p*-X-substituted-phenyl rings in **2** series are perpendicular (see dihedral angle ω_1 in Table 3 and structure **2e** in Figure 5). With the exception of **2b** (X = SMe), where λ_{\max} is 399 nm, the maximal absorption wavelengths for porphyrin **2** series are around 350 - 360 nm. It is possible that λ_{\max} for **2b** do not correspond to a Soret B band but to a β band (also called Q band). For porphyrins **3** and **4** series, the porphin chromophore and aryl group are separated by one methylene or by an ethylene group, respectively, thence absorption wavelengths are not very different from porphyrin **2** series. However, λ_{\max} for **3c**, **3e**, **4a-4c** and **4e**, is likely of a Q band not of a B band. The case of porphyrin series **5** is different since the two aromatic rings are connected by an etheno bridge, thus the observed red-shifts in λ_{\max} with respect to porphyrins series **3**

or **4** are expected, even though molecules are not totally planar (see dihedral angles ω_1 and ω_3 in Table 3 and structure **5e** in Figure 5).

As previously discussed, neither porphyrinoids **3** series nor **4** series have the two aromatic rings in a coplanar arrangement, however the λ_{\max} absorption of porphyrinoids **3** and **4** shifts dramatically to longer wavelengths with respect to their saturated porphyrin series. The bathochromic effects are summarized in Table 6 as relative $\Delta\lambda_{\max}$ wavelengths. The $\Delta\lambda_{\max}$ range values are 159 nm - 199 nm for **3** series, 165 nm - 307 nm for **4 α** , and 180 nm - 373 nm for **4 β** .

CONCLUSION

Free radical stability of porphyrinoids **3(a-h)** and **4(a-h)** was calculated by means of their isodesmic radical stabilization energy (RSE) values obtained using DFT method at the UB3LYP/6-31(Gd,p) level of theory. The pertinence of the theoretical method used here was confidently proved by linear regression of RSE values calculated for benzyl radicals **6(a-h)** with various reported radical scales.

Geometry and spin density, at the radical center and key positions of the porphin and *p*-X-substituted phenyl rings allowed spin delocalization in **3** and **4** series to be analyzed.

Although noncoplanarity of the aromatic rings is consistently found in porphyrinoids **3** and **4**, important bathochromic effects are observed when compared with their saturated porphyrin counterparts.

ACKNOWLEDGEMENTS

Financial support from Instituto de Ciencia y Tecnología del Distrito Federal (ICyTDF) through the project ICyTDF/316/2009 is greatly appreciate it.

REFERENCES

- Ali, M.E., Sanyal, B., Oppeneer, P.M. (2012) Electronic structure, spin-states, and spin-crossover reaction of heme-related Fe-porphyrins: a theoretical perspective. *Journal of Physical Chemistry B* **116** : 5849-5859
- Barragán, E., Gordillo, B., Vargas, G., Velazco, L. (2004) The role of cobalt, copper, nickel, and zinc in the DNA replication inhibitory activity of *p*-aminophenyl triphenylporphyrin. *Applied Organometallic Chemistry* **18** : 311-317
- Barragán, E., Gordillo, B., Vargas, G., Cortez, M.T., Jaramillo, B.E., Villa-Treviño, S., Fattel-Fazenda, S., Ortega, J., Velazco, L. (2005) DNA replication inhibition and fluorescence microscopy of non-cationic porphyrins in malignant cells. *Arkivoc* **VI**, 436-448
- Barragán, E., Gordillo, B., Vargas, G. (2010) Obtención y síntesis de porfirinil-nucleótidos neutros, su aplicación como pro-drogas y su uso como agentes anticancerígenos y antivirales. Patente Número PA/a/2003/011108, folio 73749, otorgada por el Instituto Mexicano de la Propiedad Industrial (IMPI)
- Barth, R.F., Coderre, J.A., Vicente, M.G.H., Blue, T.E. (2005) Boron neutron capture therapy of cancer: current status and future prospects. *Clinical Cancer Research* **11** : 3987-4002
- Creary, X. (2006) Super radical stabilizers. *Accounts of Chemical Research* **39** : 761- 771.
- Dust, J.M., Arnold, D.R. (1983) Substituent effects on benzyl radical ESR hyperfine coupling constants. The σ_a^* scale based upon spin delocalization *Journal of the American Chemical Society* **105** : 1221-1227
- Edwards, L., Dolphin, D.H., Gouterman M., Adler, A.D. (1971) Porphyrins XVII. Vapor absorption spectra and redox reactions: tetraphenylporphyrins and porphin. *Journal of Molecular Spectroscopy* **38** : 16-32
- Ishida, M., Shin, J.-Y., Lim, J.M., Lee, B.S., Yoon, M.-C., Koide, T., Sessler, J.L., Osuka, A., Kim, D. (2011) Neutral radical and singlet biradical forms of meso-free, -keto, and -diketo hexaphyrins (1.1.1.1.1.1): effects on aromaticity and photophysical properties. *Journal of the American Chemical Society* **133** : 15533-15544
- Jiang, X.-K. and Ji, G.-Z. (1992) A self-consistent and cross-checked scale of spin-delocalization substituent constants, the σ_{H}^* scale. *Journal of Organic Chemistry* **57** : 6051-6056
- Groves, J.T., McClusky, G.A., White, R.E., Coon M.J. (1978) Aliphatic hydroxylation by highly purified liver microsomal cytochrome P-450. Evidence for a carbon radical intermediate. *Biochemical and Biophysical Research Communications* **81** : 154-160
- Lin, V.S.-Y., DiMagno, S.G., Therien, M.J. (1994) Highly conjugated, acetylenyl bridged porphyrins: new models for light-harvesting antenna systems. *Science* **264** : 1105-1111
- Marsh, D.F. and Mink, L.M. (1996) Microscale synthesis and electronic absorption spectroscopy of tetraphenylporphyrin H₂(TPP) and metalloporphyrins Zn^{II}(TPP) and Ni^{II}(TPP). *Journal of Chemical Education* **73** : 1188-1190
- Meunier, B., de Visser, S.P., Shaik, S. (2004) Mechanism of oxidation reactions catalyzed by cytochrome P450 enzymes. *Chemical Reviews* **104** : 3947-3980
- Moan, J., Peng, Q., Evensen, J.F., Berg, K., Western, A., Rimmington, C. (1987) Photosensitizing efficiencies, tumor and cellular uptake of different photosensitizing drugs relevant for photodynamic therapy of cancer. *Photochemistry and Photobiology* **46** : 713-721
- Poole, R.K. and Kalnenieks, U. (2000) Introduction to light absorption: visible and ultraviolet spectra. In Gore, M.G. (ed) Spectrophotometry and spectrofluorimetry. A practical approach. Oxford University Press, GB pp. 7-8

- Pou, S., Halpern, H.J., Tsai, P., Rosen G.M. (1998) Issues pertinent to the in vivo in situ spin trapping of free radicals. *Accounts of Chemical Research* **32** : 155-161
- Reisch, M. (2012) One in 50 billion. Start-up firme Rarecyte gets in on the race to detect tumor cell in blood. *Chemical and Engineering News*, September 10, p. 21
- Rittle J. and Green M.T. (2010) Cytochrome P450 compound I: capture, characterization, and C-H bond activation kinetics. *Science* **330** : 933-937
- Scruggs, E.R. and Naylor, A.J.D. (2008) Mechanisms of zidovudine-induced mitochondrial toxicity and myopathy. *Pharmacology* **82** : 83-88
- Shkirman, S.F., Solov'ev, K.N., Kachura, T.F., Arabei, S.A., Shakovskii, E.D. (1999) Interpretation of the Soret band of porphyrins based on the polarization spectrum of N-methyltetraphenylporphin fluorescence. *Journal of Applied Spectroscopy* **66** : 68-75
- Sofia, M.J., Chang, W., Furman, P.A., Mosley, R.T., Ross, B.S. (2012) Nucleoside, nucleotide, and non-nucleoside inhibitors of hepatitis C virus NS5B RNA-dependent RNA-polymerase *Journal of Medicinal Chemistry* **55** : 2481-2531
- Wu, Y.-D., Wong, C.-L., Chan, K.W. K. (1996) Substituent effects on the C-H bond dissociation energy of toluene. A density functional study. *Journal of Organic Chemistry* **61** : 746-750